

# Water Transport and Purification in Nanochannels Controlled by Asymmetric Wettability

Qinwen Chen, Lingyi Meng, Qikai Li, Dong Wang, Wei Guo, Zhigang Shuai,\* and Lei Jiang\*

**B**iomimetic asymmetric nanochannels have recently attracted increasing attention from researchers, especially in the aspect of the asymmetric wettability (a hydrophilic–hydrophobic system), which can be utilized to control the wetting behavior of aqueous media and to offer a means for guiding water motion. By using molecular dynamics simulations, a design for a potentially efficient water filter is presented based on ( $n$ ,  $n$ ) single-walled carbon nanotubes, where  $n = 6, 8, 10$  and  $12$ , asymmetrically modified with hydrophilic groups (carboxyl,  $-\text{COOH}$ ) at one tip and hydrophobic groups (trifluoromethyl,  $-\text{CF}_3$ ) at the other. The reduced water density on the hydrophobic sides of the functionalized nanotubes are observed in both pure water and aqueous electrolyte solution, except for the functionalized (6, 6) tube, due to the change of dipole orientation of the single-file water wire within it. The functionalized (8, 8) tube can significantly maintain the low water density on the hydrophobic side. Both (6, 6) and (8, 8) tubes have relatively high energy barriers at their tips for ion permeation, which can be obtained by calculating the potential of mean force. Such tip functionalization of a nanotube therefore suggests the great possibilities of water transport and filtration, dominated by asymmetric wettability. The functionalized (8, 8) tube could act as a nanofluidic channel for water purification, not only for ion exclusion but also as a stable water column structure.

## 1. Introduction

Shortage of freshwater resources constitutes one of the major problems in the world. Drawing clean water from seawater has been a virtually inexorable trend for many years. Due to the high operating costs, tremendous amounts of researches are conducted to identify the robust new

techniques and facilities at lower cost and with less energy consumption.<sup>[1–4]</sup> Carbon nanotubes (CNTs) are considered to be the ‘simplest’ nonpolar pores.<sup>[5]</sup> The outcome of recent researches on the water transport through CNTs offer great promise, and they are being considered as nanofluidic channels for the next generation of water purification, not only because water molecules confined within the tubes present significantly different and unusual properties in contrast with molecules in the bulk, e.g., fast flow rates induced by the weak interactions between water molecules and the tube walls,<sup>[1,6–9]</sup> but also because CNTs show high selectivity for water molecules as well as a large variety of solutes,<sup>[10–14]</sup> which can dramatically reduce the amount of energy required for water purification and desalination. However, due to the intrinsic limitations of experimental procedures, many aspects concerning the directed water transfer in CNTs, to a large extent, remain yet to be explored.

This research was inspired by the stenocara beetle living in the Namib Desert: it utilizes a hydrophobic surface with

Dr. Q. W. Chen, Dr. L. Y. Meng, Dr. W. Guo, Prof. L. Jiang  
Institute of Chemistry  
Chinese Academy of Sciences  
Zhongguancun, Beijing 100190, P.R. China  
E-mail: jianglei@iccas.ac.cn

Dr. Q. K. Li, Dr. D. Wang, Prof. Z. G. Shuai  
Department of Chemistry  
Tsinghua University  
Beijing 100084, P.R. China  
E-mail: zgshuai@tsinghua.edu.cn

DOI: 10.1002/sml.201100287

a random array of hydrophilic bumps on its back to collect drinking water. Hydrophilic–hydrophobic patterned surfaces have been shown to offer a promising means for guiding water motion.<sup>[15]</sup> Scientists have extended this idea to nanochannels via chemical modification. Our group has been devoted to developing biomimetic asymmetric nanochannels.<sup>[16–18]</sup> In addition, Wang et al. observed an interesting unidirectional water transfer through fabrics induced by the asymmetric modification on two sides of the fabric membrane.<sup>[19]</sup> Recently, tip functionalization of CNTs has been the focus of both experimental and theoretical investigations, aiming at increasing both flux and selectivity of the separation processes.<sup>[20,21]</sup> Considering that the hydrophilic–hydrophobic system can be utilized to control the wetting behavior of aqueous media, there is a demand to extensively study water transport through such functionalized nanotubes as induced by asymmetric wettability.

The uncapped armchair single-walled carbon nanotubes (SWNTs) have been used as an ideal model to investigate water and solute transport in nanochannels.<sup>[5,6,22,23]</sup> A chemical potential difference between the two sides of the channel in the form of osmotic or hydrostatic pressure gradients is widely used to determine the permeability of a water channel, in much the same way as in the design of an osmotic or reverse-osmotic force.<sup>[24–26]</sup> Recently, it has been shown that a net water transport in SWNTs can be obtained, attributed to rotation–translation coupling of the water molecules by applying an electric field or by attaching chemical functional groups at the tube tips.<sup>[27]</sup> Gong et al. observed a continuous unidirectional water flow by putting a series of point charges adjacent to the nanopore.<sup>[28]</sup> Joseph et al. predicted that the charged chemical groups at the entrance to the CNT core could affect ion transport through the nanotube, dominated by electrostatic interactions.<sup>[29]</sup> Corry investigated water and ion transport through the 1.1 nm-diameter nanotubes and modified with a variety of charged and polar functional groups, showing the implications of achieving salt rejection and rapid water flow.<sup>[30]</sup> In spite of the numerous attempts to exploit the potential transport properties of nanochannels, the wettability gradient has received little attention, and so a theoretical investigation for tip-functionalized nanotubes with asymmetric modifications is thus necessary as it can help us understand the impact of the hydrophilic–hydrophobic system on water transport and design novel nanofluidic devices with desired properties.

In this paper, we choose the finite-length ( $n, n$ ) SWNTs, which are tip-modified with hydrophilic groups and hydrophobic groups at respective tips, to test water and ion transport through these tubes. A reduced water density is found at the hydrophobic side of all tubes in pure water environments due to asymmetrical tip-functionalization. However, in

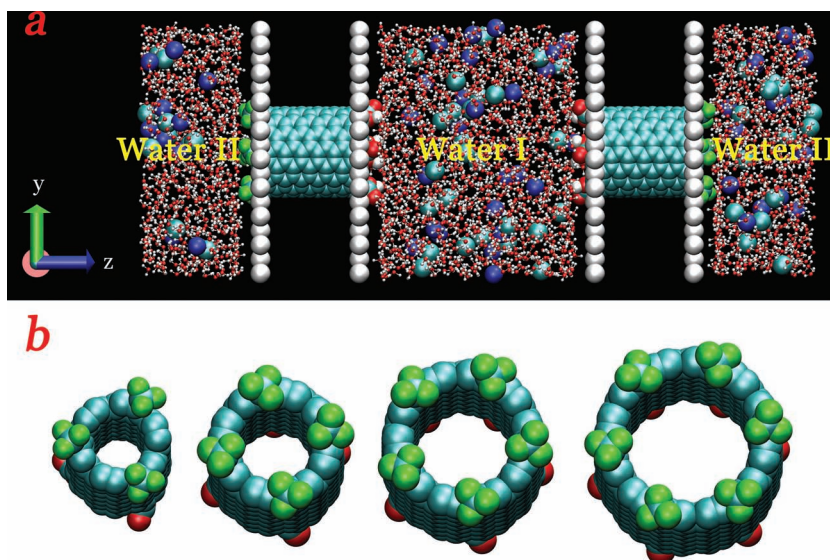


**Figure 1.** a) Schematic of the simulation set-up. b) Top views of the four ( $n, n$ ) SWNTs tip-modified with  $-\text{CF}_3$  groups (green) and  $-\text{COOH}$  groups (red), aligning from left to right: (6, 6), (8, 8), (10, 10), and (12, 12).

electrolyte solution, this density distinction on the two sides is weakened for the functionalized (6, 6) tube and is enhanced for the (8, 8) one. Neither tube allows the entrance of sodium or chloride ions due to high energy barriers at the tips, and the (8, 8) tube is considered as a potentially efficient water filter in electrolyte solutions. For the relatively wider (10, 10) and (12, 12) tubes, ions are observed to permeate to the side with low water density. This theoretical study facilitates the further exploration of the potential application of tip-functionalized SWNTs to desalination and water purification.

## 2. Model and Computational Details

**Figure 1a** shows the set-up of our simulation model which consists of two asymmetrically functionalized SWNTs, four slabs composed of pseudo atoms, water molecules and ions. To investigate the effects of the substituting groups on water transport, this model is designed as a sandwich-type to facilitate us to distinguish two water environments (waters I and II). The uncapped armchair SWNTs with a length of  $14.8 \text{ \AA}$  are modified with hydrophilic groups (carboxyl group,  $-\text{COOH}$ ) and hydrophobic groups (trifluoromethyl group,  $-\text{CF}_3$ ) at the two tips (Figure 1b). The SWNTs with  $n = 6, 8, 10,$  and  $12$  are shown to have diameters of  $8.1, 10.9, 13.6,$  and  $16.3 \text{ \AA}$ , respectively. Water I is sandwiched between the hydrophilic tips of the two SWNTs while water II is sandwiched between the two hydrophobic tips, as shown in Figure 1a. The bulk contains approximately 2786 water molecules (the sum of waters I and II) for the pure water environment, and 52 sodium and chloride ion pairs replacing around 150 water molecules for the  $1.0 \text{ M}$  solution environment. The initial quantity of water molecules and ions on one side is set to be equal to that on the other side, and about 10–140 water

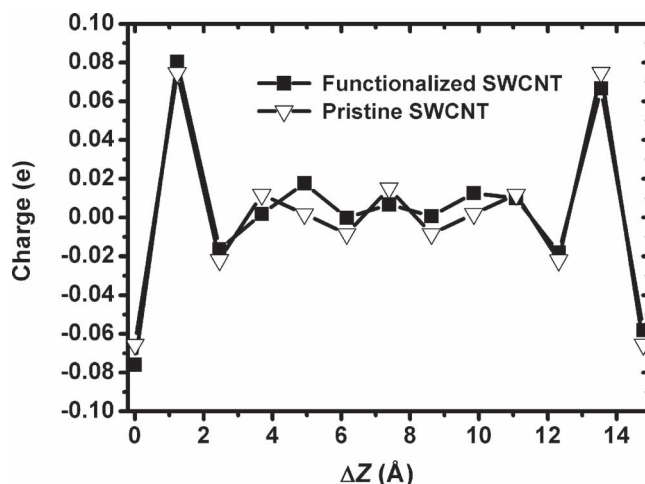
**Table 1.** Partial charges for all atoms and parameters for all van der Waals' interactions between atoms.

	Sites	$\sigma$ [Å]	$\epsilon$ [kcal mol <sup>-1</sup> ]	$q$ [e <sup>-</sup> ]
Nanotube	CB	3.361	0.0970	See Figure 2
	C (-COOH)	3.361	0.0970	0.7286
	O (carbonyl)	2.626	0.4122	-0.5696
	O (hydroxyl)	2.955	0.0002	-0.6641
	H	0	0	0.4595
	C (-CF <sub>3</sub> )	3.361	0.0970	-0.6243
	F	3.843	0.0015	-0.2298
Slab	Pseudo Atom	3.871	0.0012	0
Water	OW	3.165	0.1554	-0.8476
	HW	0	0	0.4238
Ion	Sodium	2.575	0.0148	1.0
	Chloride	4.448	0.1065	-1.0

molecules are initially placed inside the nanotubes depending on the diameters of nanotubes. The DFT calculations made with the Gaussian 03 program<sup>[31]</sup> are carried out using the hybrid B3LYP functional<sup>[32,33]</sup> and the 6-31G(d,p) basis set to obtain the optimized geometry for both pristine and the functionalized (6, 6) tubes, and the atomic partial charges with the CHELPG scheme for electrostatic potential fitting.<sup>[34]</sup> The charges are then averaged for graphite carbons with the same axial position. Considering the similar trend of charge distribution with the increasing diameter of the tubes, the averaged charges are also assigned to the graphite carbons with the corresponding axial position in functionalized (8, 8), (10, 10), and (12, 12) tubes. **Table 1** lists the partial charges for all atoms and the parameters for all van der Waals' interactions between atoms, taken from the GROMOS96 force-field.<sup>[35,36]</sup> The partial charges of graphite carbons of pristine and functionalized (6, 6) tubes show little difference, but the charge distribution of the latter is found to be asymmetric under the influence of functional groups (**Figure 2**). When combining with the effect of chemical groups, an electric field along the nanotube axis is thus generated.

The extended simple point charge (SPC/E) model<sup>[37]</sup> is used to describe the water–water interactions in pure water and also in the electrolyte solutions. The ions are treated as the charged Lennard–Jones (L–J) sites. The electrostatic interactions are evaluated by the particle mesh Ewald method using splines of order 4 with a 10–5 tolerance. The cutoff distances for the short-range Coulomb potential and L–J potential are 9.0 Å and 10.0 Å, respectively.

The SWNT–water/solution system is simulated using the canonical NVT ensemble. The box dimensions are  $L_x = 37.0$  Å,  $L_y = 37.0$  Å, and  $L_z = 100.0$  Å.  $z = 0$  corresponds to the left end of the box, as shown in Figure 1a. Periodic boundary conditions are applied in all three dimensions. The temperature is maintained at 300 K using the Berendsen thermostat. The equations of motion are integrated by using a leapfrog Verlet algorithm and a time step of 2.0 fs is used. After a 5 ns equilibration, the simulations are continued for another

**Figure 2.** Partial charge distribution on graphite atoms of the pristine and asymmetrically functionalized SWNTs. The hydrophobic and hydrophilic groups are attached to the left and right tips respectively, see Table 1 for details.

10–40 ns to obtain enough statistical samplings to calculate the transport properties. All molecular dynamics (MD) simulations are performed with the GROMACS-3.3 software package.<sup>[36]</sup>

The potential of mean force (PMF) along the nanotube axis for water transport is calculated by integration of the average forces acting on a single water molecule,

$$W(z) - W(z_0) = \int_{z_0}^z \langle F(z') \rangle dz' \quad (1)$$

with  $z_0$  being the reference position where the PMF is zero.<sup>[9]</sup> This allows us to qualitatively assess the energy barrier for water molecules to permeate through nanotubes with different sizes. The profiles of the individual components of PMF do not necessarily reflect free energies, and can only be interpreted qualitatively.

The PMFs for ions passing through the functionalized SWNTs are determined using umbrella sampling<sup>[38]</sup> by applying a harmonic biasing potential  $(K_{x,i}/2)(x-x_i)^2 + (K_{y,i}/2)(y-y_i)^2 + (K_{z,i}/2)(z-z_i)^2$  on a test ion, where the  $x$ ,  $y$ , and  $z$  are the real-time coordinates of the ion, the  $x_i$ ,  $y_i$ , and  $z_i$  are target positions in the  $i$ th umbrella-sampling window, and the  $K_{x,i}$ ,  $K_{y,i}$ , and  $K_{z,i}$  are the corresponding force constants. The target position is moved from outside to inside the nanotube along the central axis ( $x_i = y_i = 18.5$  Å) with 0.5 Å increments. For the functionalized (6, 6) tube, the  $K_{z,i}$  of 10.0 kcal mol<sup>-1</sup>Å<sup>-2</sup> is applied to the  $z_i$  windows near the tube mouths and that of 5.0 kcal mol<sup>-1</sup>Å<sup>-2</sup> is used for the remaining windows, correspondingly  $K_{x,i}$  and  $K_{y,i}$  of 5.0 kcal mol<sup>-1</sup>Å<sup>-2</sup> are used for all windows. For the other nanotubes, the  $K_{x,i}$ ,  $K_{y,i}$ , and  $K_{z,i}$  of 5.0 kcal mol<sup>-1</sup>Å<sup>-2</sup> are used. Each window is sampled with 600 ps and the coordinates of the test ion are written every 5 fs, and the samplings for the last 300 ps of each run are recorded for collective analysis of the data using the weighted histogram analysis method (WHAM).<sup>[39,40]</sup>

### 3. Results and Discussion

#### 3.1. Water Transport in Pristine and Functionalized SWNTs

The structure and transport properties of the single-file hydrogen-bonded water wire have been demonstrated in highly confined nanopores where each water molecule acts as both donor and acceptor to generate hydrogen bonds between its neighbors, such as in some pristine nanotubes and biological water channels. Furthermore, the asymmetric modification of nanotubes is expected to achieve a water-driving mechanism induced by chemical potential gradient. That is, it is expected that the fine structure and dynamical behavior of water molecules in these channels can be altered. The carboxyl group is well known as a hydrophilic group, including both hydrogen-bond acceptor and donor, while the hydrophobic feature is usually acquired by fluorinated groups (e.g., the trifluoromethyl group). These groups can form hydrophilic and hydrophobic networks respectively in water, resulting in the local rearrangement of the layout for hydrogen bonds. Accordingly, carboxyl and trifluoromethyl groups are selected to modify the two tips of the nanotubes. **Figure 3** shows the comparison of water transport in the pristine and functionalized (6, 6) tubes under equilibrium condition.  $\rho(t)$  is the water density as a function of time. It is observed that  $\rho(t)$  for the waters I and II exhibits frequent overlap in pristine tubes, but a distinguishable difference in asymmetric tubes. A reduced water density is found on the hydrophobic side of the tube (water II), indicating that water tends to transfer from the hydrophobic side of the nanotube to the hydrophilic side, to achieve a balanced chemical potential of the hydrophilic–hydrophobic system, and finally form stable density distribution. The fluctuation of water density is also attributed to the fluctuation of the number of waters occupying the nanotube. As reported earlier,<sup>[22]</sup> the energy barrier for water molecules to transport through SWNTs can be calculated by using the PMF method. The symmetrical and asymmetrical energy barriers for water transport are observed in the pristine and functionalized (6, 6) tubes, respectively, from the PMFs shown in **Figure 3**. Note that only the PMFs for  $z = 0\text{--}50.0 \text{ \AA}$  are shown in the figure due to the symmetric nature of the model system. The energy barrier at the hydrophilic tip is slightly higher than that at the hydrophobic one, and the reason is possibly that free energy of the hydrophilic interaction is greater than that of the hydrophobic attraction due to the omnipresent hydrogen-bonding free energy of cohesion of water.<sup>[41]</sup> The orientation dipole of a water molecule inside the nanotube is defined relative to the nanotube axis. In the pristine nanotube, all the water molecules are oriented towards either tip of the nanotube. However, the waters at the two tips of the functionalized nanotube exhibit the opposite orientation, with dipole orientations consistently pointing towards

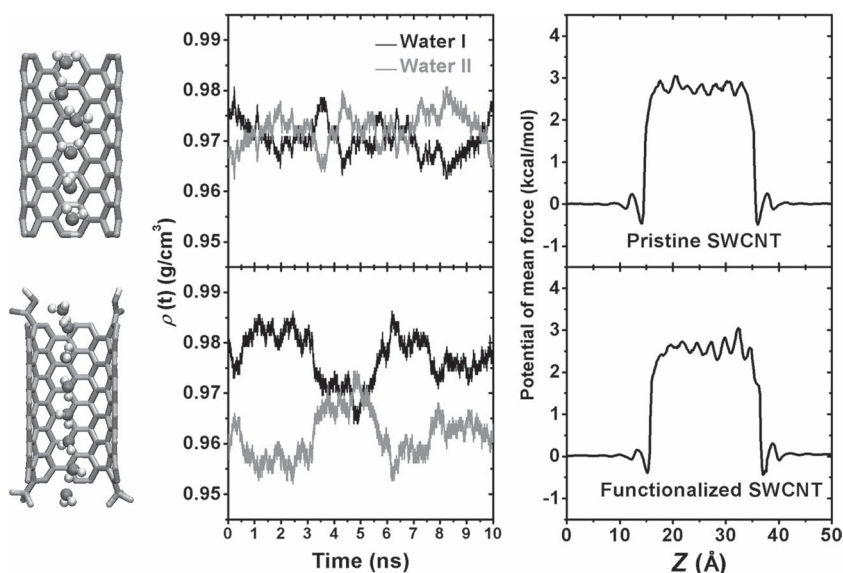


**Figure 3.** Comparison of water transport through the pristine and functionalized (6, 6) tubes in pure water.

the outside of the tube (**Figure 3**), as a result of the dominant electrostatic coupling between the water molecules and substituting groups, since a strong electrostatic field is generated by carboxyl groups as well as trifluoromethyl groups at the tips of the nanotube. According to the coupling mechanism of the rotational and translational degrees of freedom responsible for water transport through the nanotube,<sup>[27]</sup> the total electric field along the nanotube axis induced by asymmetric partial charge distribution provides a good driving force for directional water-transfer through nanotubes.

**Figure 4** shows the results for water transport in the functionalized (8, 8), (10, 10), and (12, 12) tubes under equilibrium condition. In contrast to the functionalized (6, 6) tube, the new energy barriers appear at  $z \approx 15.0$  and  $36.0 \text{ \AA}$  in the (8, 8) tube because of the increased electrostatic coupling between the groups and water molecules. The structure of the four water columns in the (8, 8) tube is much like that in the unsubstituted one.<sup>[42,43]</sup> The dipole orientations of water molecules at the two tips of the nanotube are opposite to each other and point towards outside of the tube. The decreased energy barrier, and less density distinctions between waters I and II, are also observed in the (10, 10) and (12, 12) tubes, suggesting that the effects of chemical modification are weakened with increasing nanotube diameters.

#### 3.2. Water Transport and Purification in Functionalized SWNTs

To test the influence of the hydrophilic–hydrophobic system on water transport in an electrolyte solution, 1 M NaCl solution instead of pure water environment was used. **Figure 5** shows the results for water transport in the four asymmetrically functionalized SWNTs mentioned above. It is obvious that the density distinction between waters I and II is greatly weakened for the (6, 6) tube in solution compared with that in pure water. Also, an enhanced and stable periodic

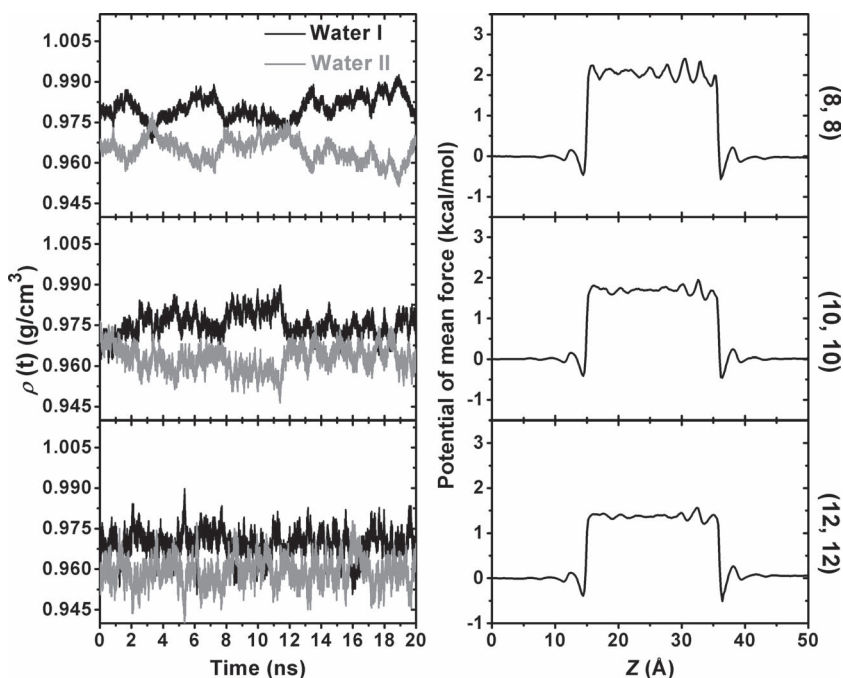


Figure 4. Water transport through the functionalized (8, 8), (10, 10), and (12, 12) tubes in pure water.

density distinction is observed in the (8, 8) tube. The PMFs for water transport exhibit no obvious difference from those calculated in pure water, except for the (6, 6) tube where a shift of the position of the free-energy barrier is observed at the hydrophilic tip. Considering that the orientation dipoles of water molecules can be strongly affected by the electrostatic interactions,<sup>[22]</sup> the water molecule dipole confined within the (6, 6) tube both in pure water and electrolyte solution are carefully investigated. **Figure 6** shows the distribution of dipole orientations for water molecules within the 40 ns simulation under equilibrium conditions. Three window positions are chosen, located at  $z = 17.0\text{--}18.8\text{ \AA}$  (hydrophobic tip),  $24.5\text{--}28.3\text{ \AA}$  (middle), and  $29.9\text{--}31.7\text{ \AA}$  (hydrophilic tip). It is shown that the highest-angle dipole distribution at the hydrophobic tip is around  $162^\circ$  in pure water and  $157^\circ$  in solution, while at the hydrophilic tip it is around  $18^\circ$  in pure water and  $30^\circ$  in solution. The dipole orientation for water molecules in the middle of the nanotube exhibits a high distribution at  $40^\circ$ ,  $90^\circ$ , and  $145^\circ$ , and the peaks get stronger with increasing dipole angle in pure water, while tending to be equivalent in solution. The existence of ions in the bulk greatly affects the dipole-dipole and hydrogen-bonding interactions of water molecules, and this effect is prominent in the (6, 6) tube due to the structure of the single-file water wire within it, leading to changes in amplitude and frequency of water density

lines and weakening the density distinction for the two sides of the tube. However, for the water molecules confined within the (8, 8) tube in solution environment, highly ordered structure of the four-water columns looks much like the one in the pure water. Thus, there are no notable changes in water PMF and the water density distinction is still remarkable.

The functionalized SWNTs offer potential water filters for wastewater reuse and seawater desalination applications. As a result, it is necessary to assess free-energy barriers for the ions to pass through the functionalized nanotubes. The energy barriers for ions entering pristine SWNTs have captivated the interest of many theorists, who have predicted that sodium and chloride ions face a large energy barrier and they can not pass through the narrow (6, 6) tube but can pass through the wider (8, 8) tube.<sup>[11]</sup> It is suspected that these conclusions could be altered as the nanotubes are modified by functional chemical groups. Our results show that no ion permeation is found in the functionalized

(6, 6) and (8, 8) tubes during the whole simulation time. The umbrella sampling method is thus applied to investigate the likelihood of ions passing through the nanotubes by moving a test ion from outside to inside the nanotube. **Figure 7** shows the PMF curves for the ion to pass through the functionalized (6, 6), (8, 8), and (10, 10) tubes. Assuming that the position of the slab is  $\Delta z = 0$ , the ion will move by  $13.5\text{ \AA}$  from bulk to the slab and continue moving by  $2.5\text{ \AA}$  from the slab

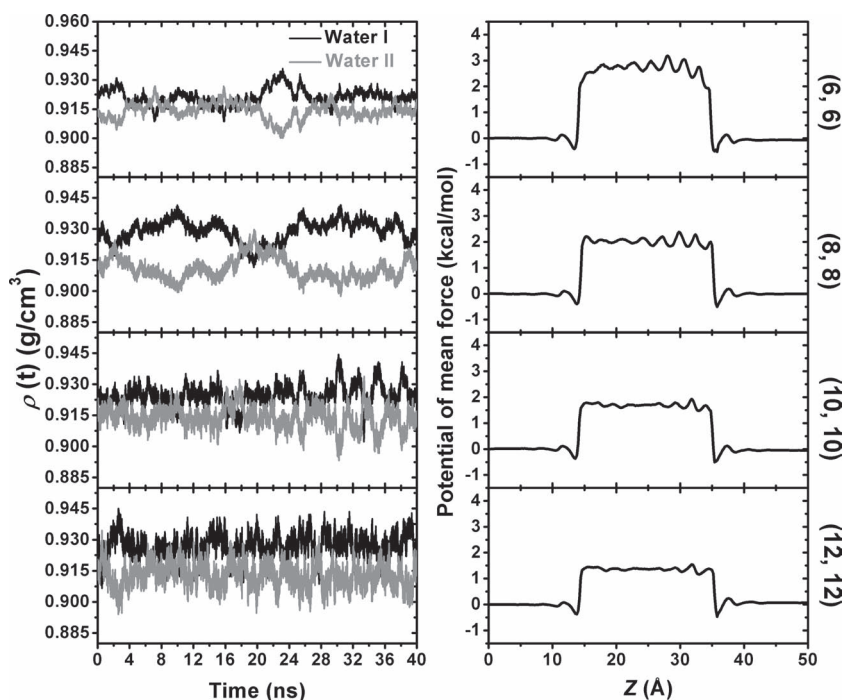
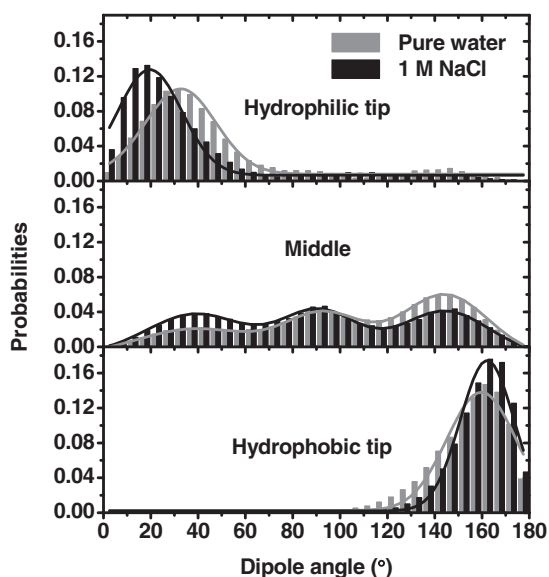
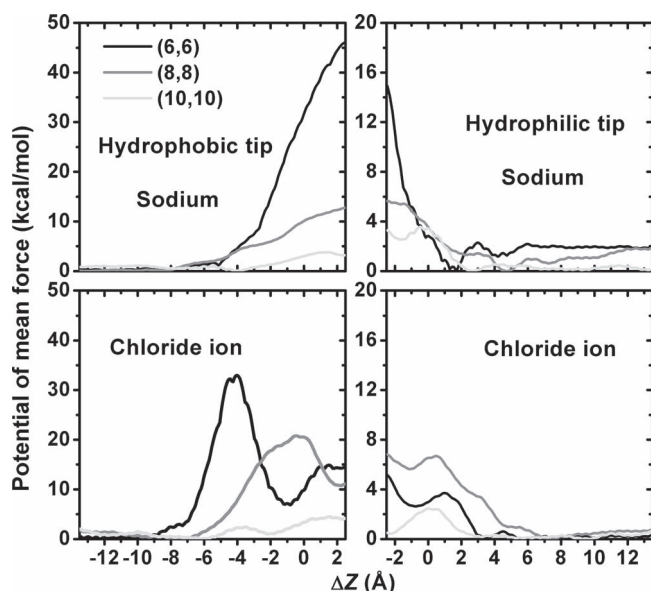


Figure 5. Water transport through the functionalized tubes in 1.0 M NaCl solution.



**Figure 6.** Water dipole orientation in the functionalized (6, 6) tubes in pure water versus in NaCl solution. The top, middle, and bottom panels represent the orientation of water molecules located at  $z = 17.0\text{--}18.8\text{ \AA}$  (hydrophobic tip),  $24.5\text{--}28.3\text{ \AA}$  (middle), and  $29.9\text{--}31.7\text{ \AA}$  (hydrophilic tip). The orientation dipole is defined relative to the positive  $z$  axis.

to inside the nanotube. Our results show that the energy barrier at the hydrophobic tip is much higher than that at the hydrophilic tip for both sodium and chloride ions. There exist very high free-energy barriers for the sodium and chloride ions to permeate through the functionalized (6, 6) tube. For the (8, 8) tube, the free-energy barriers for ions are still kept more than  $10\text{ kcal mol}^{-1}$  due to the tip modification. High-



**Figure 7.** Potential of mean force for sodium and chloride ions to permeate into the functionalized tubes. Assuming that the position of the slab at both hydrophobic and hydrophilic tips is  $\Delta z = 0$ , the ion will move by  $13.5\text{ \AA}$  from bulk to the slab and continue moving by  $2.5\text{ \AA}$  from the slab to inside the nanotube.

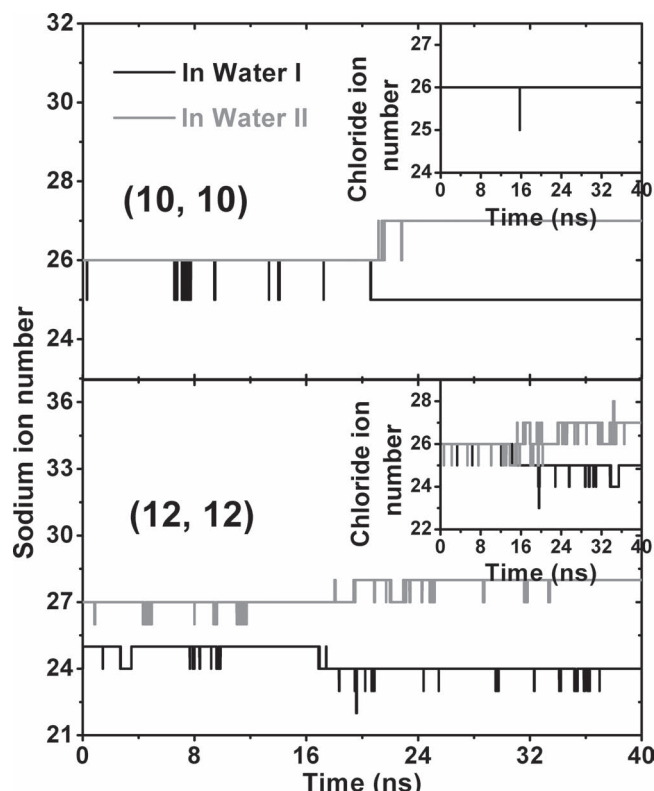


**Figure 8.** The ion number fluctuation in water I and water II for the functionalized (10, 10) and (12, 12) tubes under equilibrium conditions.

energy barriers in the region of chemical groups in the PMFs for chloride are due to the negative–negative electrostatic repulsion between the chloride ion and the carboxyl as well as trifluoromethyl groups. As the tube diameter is increased, the energy barriers decrease to below  $5\text{ kcal mol}^{-1}$  in the (10, 10) nanotube, which is slightly higher than the barriers for water entering nanotubes, and the ions passing through the nanotubes are identified. **Figure 8** shows the number of ions as a function of time in the water I and the water II areas after 10 ns of equilibration. In the (10, 10) tube, only one sodium ion is found to be transferred from the hydrophilic tip to the hydrophobic tip, and the chloride ion seems to be favorable in the bulk. Similarly, it is observed that two sodium and two chloride ions permeate through the (12, 12) tube. Finally, a stable concentration distinction is maintained by the asymmetrically tip-functionalized carbon nanotubes.

#### 4. Conclusion

Inspired by nature, we have extended and designed tip-functionalized SWNTs controlled by asymmetric wettability. The hydrophilic–hydrophobic system presents a significant step for the directional water transport. It is found that there exists a stable water density distinction between the water I and II areas under equilibrium conditions. No ion permeation is found in the functionalized (6, 6) and (8, 8) tubes due to large free-energy barriers at their mouths, based on the PMF

calculations. Less difference in the water density across the functionalized (6, 6) tube in electrolyte solution is found than in pure water due to the change of dipole orientation of the single-file water wire within it. The functionalized (8, 8) tube, with a highly ordered structure of four water columns within it, can well maintain the low water density at the hydrophobic side, simultaneously excluding sodium and chloride ions, and thus act as a potentially efficient water filter. For the functionalized (10, 10) and (12, 12) tubes, ions were transported from the hydrophilic side to the hydrophobic side to achieve a balanced chemical potential across the nanotubes. We conclude that coupling the asymmetrically tip-functionalized carbon nanotubes with hydrophobic and hydrophilic groups offers excellent opportunities not only in desalination for water purification but also in the utilization of carbon nanotubes for various nanofluidic devices.

## Acknowledgements

Dr. Q. W. Chen would like to thank Prof. Y. Q. Gao, Dr. Y. L. Niu, Dr. Z. Y. Ma and J. M. Chen for helpful discussions and advice. This work has been supported by National Research Fund for Fundamental Key Projects (2011CB935703, 2010CB934700, 2009CB930404, 2007CB936403), National Natural Science Foundation (20773145, 20920102036, 20974113), as well as the Chinese Academy of Sciences including its CNIC supercomputing center.

- [1] R. F. Service, *Science* **2006**, *313*, 1088.
- [2] A. Noy, H. G. Park, F. Fornasiero, J. K. Holt, C. P. Grigoropoulos, O. Bakajin, *Nano Today* **2007**, *2*, 22.
- [3] M. A. Shannon, P. W. Bohn, M. Elimelech, J. G. Georgiadis, B. J. Marinas, A. M. Mayes, *Nature* **2008**, *452*, 301.
- [4] S. J. Kim, S. H. Ko, K. H. Kang, J. Han, *Nat. Nanotechnol.* **2010**, *5*, 297.
- [5] G. Hummer, *Mol. Phys.* **2007**, *105*, 201.
- [6] G. Hummer, J. C. Rasaiah, J. P. Noworyta, *Nature* **2001**, *414*, 188.
- [7] M. Majumder, N. Chopra, R. Andrews, B. Hinds, *Nature* **2005**, *438*, 44.
- [8] S. Joseph, N. R. Aluru, *Nano Lett.* **2008**, *8*, 452.
- [9] L. Meng, Q. Li, Z. Shuai, *J. Chem. Phys.* **2008**, *128*, 134703.
- [10] A. Srivastava, O. N. Srivastava, S. Talapatra, R. Vajai, P. M. Ajayan, *Nat. Mater.* **2004**, *3*, 610.
- [11] B. Corry, *J. Phys. Chem. B* **2008**, *112*, 1427.
- [12] C. Song, B. Corry, *J. Phys. Chem. B* **2009**, *113*, 7642.
- [13] A. K. Mishra, S. Ramaprabhu, *J. Phys. Chem. C* **2010**, *114*, 2583.
- [14] Miao Yu, Hans H. Funke, John L. Falconer, R. D. Noble, *J. Am. Chem. Soc.* **2010**, *132*, 8285.
- [15] A. R. Parker, C. R. Lawrence, *Nature* **2001**, *414*, 188.
- [16] X. Hou, H. Dong, D. Zhu, L. Jiang, *Small* **2010**, *6*, 361.
- [17] X. Hou, Y. Liu, H. Dong, F. Yang, L. Li, L. Jiang, *Adv. Mater.* **2010**, *22*, 2440.
- [18] X. Hou, F. Yang, L. Li, Y. Song, L. Jiang, D. Zhu, *J. Am. Chem. Soc.* **2010**, *132*, 11736.
- [19] H. Wang, J. Ding, L. Dai, X. Wang, T. Lin, *J. Mater. Chem.* **2010**, *20*, 7938.
- [20] M. Majumder, N. Chopra, B. J. Hinds, *J. Am. Chem. Soc.* **2005**, *127*, 9062.
- [21] F. Fornasiero, H. G. Park, J. K. Holt, M. Stadermann, C. P. Grigoropoulos, A. Noy, O. Bakajin, *Proc. Natl. Acad. Sci. USA* **2008**, *105*, 17250.
- [22] C. Y. Won, S. Joseph, N. R. Aluru, *J. Chem. Phys.* **2006**, *125*, 114701.
- [23] H. Fang, R. Wan, X. Gong, H. Lu, S. Li, *J. Phys. D: Appl. Phys.* **2008**, *41*, 103002.
- [24] A. Kalra, S. Garde, G. Hummer, *Proc. Natl. Acad. Sci. USA* **2003**, *100*, 10175.
- [25] F. Zhu, E. Tajkhorshid, K. Schulten, *Phys. Rev. Lett.* **2004**, *93*, 224501.
- [26] M. E. Suk, N. R. Aluru, *Phys. Chem. Chem. Phys.* **2009**, *11*, 8614.
- [27] S. Joseph, N. R. Aluru, *Phys. Rev. Lett.* **2008**, *101*, 064502.
- [28] X. Gong, J. Li, H. Lu, R. Wan, J. Li, J. Hu, H. Fang, *Nat. Nanotechnol.* **2007**, *2*, 709.
- [29] S. Joseph, R. J. Mashl, E. Jakobsson, N. R. Aluru, *Nano Lett.* **2003**, *3*, 1399.
- [30] B. Corry, *Energy Environ. Sci.* **2011**, *4*, 751.
- [31] G. W. T. M. J. Frisch, H. B. Schlegel, G. E. Scuseria, J. R. C. M. A. Robb, J. A. Montgomery Jr., T. Vreven, J. C. B. K. N. Kudin, J. M. Millam, S. S. Iyengar, J. Tomasi, B. M. V. Barone, M. Cossi, G. Scalmani, N. Rega, H. N. G. A. Petersson, M. Hada, M. Ehara, K. Toyota, J. H. R. Fukuda, M. Ishida, T. Nakajima, Y. Honda, O. Kitao, M. K. H. Nakai, X. Li, J. E. Knox, H. P. Hratchian, J. B. Cross, C. A. V. Bakken, J. Jaramillo, R. Gomperts, R. E. Stratmann, A. J. A. O. Yazyev, R. Cammi, C. Pomelli, J. W. Ochterski, K. M. P. Y. Ayala, G. A. Voth, P. Salvador, J. J. Dannenberg, S. D. V. G. Zakrzewski, A. D. Daniels, M. C. Strain, D. K. M. O. Farkas, A. D. Rabuck, K. Raghavachari, J. V. O. J. B. Foresman, Q. Cui, A. G. Baboul, S. Clifford, B. B. S. J. Cioslowski, G. Liu, A. Liashenko, P. Piskorz, R. L. M. I. Komaromi, D. J. Fox, T. Keith, M. A. Al-Laham, A. N. C. Y. Peng, M. Challacombe, P. M. W. Gill, W. C. B. Johnson, M. W. Wong, C. Gonzalez, J. A. Pople, I. Gaussian, Wallingford CT, Gaussian 03, Revision E.01 **2003**.
- [32] A. D. Becke, *J. Phys. Chem.* **1993**, *98*, 5648.
- [33] C. Lee, W. Yang, R. G. Parr, *Phys. Rev. B* **1988**, *37*, 785.
- [34] C. M. Breneman, K. B. Wiberg, *J. Comp. Chem.* **1990**, *11*, 361.
- [35] E. Lindahl, B. Hess, D. Van Der Spoel, *J. Mol. Model.* **2001**, *7*, 306.
- [36] D. Van Der Spoel, E. Lindahl, B. Hess, A. R. van Buuren, E. Apol, P. J. Meulenhoff, D. P. Tieleman, A. L. T. M. Sijbers, K. A. Feenstra, R. v. Drunen, H. J. C. Berendsen, Gromacs User Manual version 3.3 **2005**.
- [37] H. J. C. Berendsen, J. R. Grigera, T. P. Straatsma, *J. Phys. Chem.* **1987**, *91*, 6269.
- [38] G. Torrie, J. Valleau, *Chem. Phys. Lett.* **1974**, *28*, 578.
- [39] S. Kumar, J. M. Rosenberg, D. Bouzida, R. H. Swendsen, P. A. Kollman, *J. Comp. Chem.* **1992**, *13*, 1011.
- [40] A. Grossfield, WHAM: The Weighted Histogram Analysis Method, <http://membrane.urmc.rochester.edu/content/wham>, (accessed October **2010**).
- [41] C. J. van Oss, *J. Mol. Recognit.* **2003**, *16*, 177.
- [42] W. H. Noon, K. D. Ausman, R. E. Smalley, J. Ma, *Chem. Phys. Lett.* **2002**, *355*, 445.
- [43] R. J. Mashl, S. Joseph, N. R. Aluru, E. Jakobsson, *Nano Lett.* **2003**, *3*, 589.

Received: February 9, 2011  
Published online: May 24, 2011